

## **FRACTURE AND MICROSTRUCTURAL STUDIES ON NORMAL AND HIGH STRENGTH CONCRETES WITH DIFFERENT TYPES OF AGGREGATES**

**OZKAN SENGUL, CENGIZ SENGUL, GULDEN KESKIN, YILMAZ AKKAYA,  
CANAN TASDEMIR AND MEHMET A. TASDEMIR**

Istanbul Technical University  
Civil Engineering Faculty, Istanbul, Turkey  
e-mail: tasdemirme@itu.edu.tr, www.itu.edu.tr

**Key words:** Aggregate type, Mechanical behavior, Fracture energy, Microstructural examination

**Abstract:** Effects of aggregate type on the mechanical behavior of both normal- and high-strength concretes were investigated under bending and mechanical properties under compression. Basalt, sandstone, Eocene and Devonian crushed limestone coarse aggregates were used in the concrete mixtures. For each coarse aggregate type, normal and high strength concretes were made with the same Portland cement and natural sand. In each concrete class, effective water/cement ratio, grading of aggregate, maximum particle size, and cement content were kept constant. For better understanding of the crack initiation and propagation in concretes with different coarse aggregates, a microstructural examination using optical fluorescence and SEM studies are also presented. The results obtained help to explain how the coarse aggregate type and strength of concrete affect the fracture energy in bending. Good agreement was found between experiments and a three phase composite material model previously proposed.

### **1 INTRODUCTION**

Since approximately 75 percent of the concrete volume is occupied by aggregate, the properties of aggregate greatly affect the structural performance of concrete. Several properties of aggregate such as chemical and mineral composition, structure, fabric, shape, roughness, degree of weathering, specific gravity, hardness, strength, physical and chemical stability and pore structure depend on the properties of parent rock [1-3]. All these properties may have a significant effect on the quality of concrete.

In recent years, several researchers investigated the effects of aggregate type on the mechanical properties of concrete [4-6] especially for high strength concrete, but there is little information about both microstructural and fracture properties of these concretes.

The main objective of the study presented

herein is to investigate the effects of aggregate type on the mechanical behaviour and microstructural properties of both normal- and high-strength concretes. Four crushed stone aggregates having different mineralogical compositions; basalt, sandstone, Eocene and Devonian limestone aggregates were used in the concrete mixtures. For each aggregate type, normal strength and high strength concretes were made with the same cement and natural sand. In each concrete class; effective water/cement ratio, maximum particle size, grading of aggregates and cement content were kept constant. Compressive strength, elastic modulus, splitting strength and fracture energy under bending were obtained. Microstructural investigations were also performed for better understanding the crack propagation under these two loading conditions.

## 2 EXPERIMENTAL DETAILS

### 2.1 Materials

A local natural sand of 0-2 mm and CEM I 42.5/R type cement were used in all mixtures. The silica fume (96 percent SiO<sub>2</sub> content) used in HSCs, was 10 percent by weight of cement. A polycarboxylic-ether based superplasticizer was used in low water/cement concretes to maintain equivalent slumps.

#### 2.1.1 Characteristics of coarse aggregates

Eocene and Devonian limestones, sandstone, and basalt coarse aggregates were used in the concretes. Each type of crushed aggregate was in three different sizes; crushed stone sand (0-4 mm), and coarse aggregates No.I (4-16 mm) and No.II (8-32 mm). Some physical properties of the coarse aggregates are shown in Table 1. The natural sand (0-4 mm) used has a density of 2.61 g/cm<sup>3</sup> and water absorption of 1.1%.

**Table 1.** Some physical properties of the coarse aggregates

Aggregate type	Coarse aggregate fraction, mm	Particle density (gr/cm <sup>3</sup> )	Water absorption (%)
Eocene limestone	0-4	2.61	1.9
	4-16	2.59	1.8
	8-32	2.61	1.6
Devonian limestone	0-4	2.70	1.2
	4-16	2.70	0.7
	8-32	2.71	0.4
Sandstone	0-4	2.71	0.8
	4-16	2.71	0.5
	8-32	2.72	0.5
Basalt	0-4	2.90	1.0
	4-16	2.91	0.6
	8-32	2.92	0.5

The mineralogical examinations of aggregates used can be summarized as follows:

**Basalt:** Phenocrysts in the rock consists of plagioclase, pyroxene, olivine and opaque minerals. Some of the particles contains higher amount of iron oxides.

**Eocene Limestone:** This is a porous, white colored bio-micritic rock consisting fossil particles, secondary quartz and pyrite. Secondary calcite and dolomite were observed on some particles.

**Devonian Limestone:** The rock consists of fossil particles, secondary quartz and pyrite. Some particles are porous and colored with organic materials. Secondary calcite and dolomite were observed on some particles.

**Sandstone:** The rock is consisting of quartz, feldspar, muscovite. It has generally medium sized grains but small and large size grains also exist.

Table 2 shows the chemical compositions of the aggregates used in the study.

**Table 2.** Chemical composition of aggregates, by weight

	Eocene Limestone	Devonian Limestone	Sandstone	Basalt	Sand
CaO	47.56	55.12	4.14	12.51	4.88
SiO <sub>2</sub>	4.66	0.78	56.77	44.47	87.60
Al <sub>2</sub> O <sub>3</sub>	1.12	0.25	11.61	8.47	3.21
Fe <sub>2</sub> O <sub>3</sub>	0.64	0.22	7.35	7.91	0.69
MgO	3.03	0.36	4.00	9.98	0.19
K <sub>2</sub> O	0.38	0.00	0.38	0.17	1.76
Na <sub>2</sub> O	0.15	0.00	1.89	2.08	0.93
TiO <sub>2</sub>	0.11	0.07	1.08	1.93	0.12
SO <sub>3</sub>	0.04	0.04	0.16	0.06	0.29
Loss on ignition	42.02	41.96	5.11	3.31	-

In order to determine the compressive strength and modulus of elasticity of each aggregate type, 30x60 mm drilled cores taken from rock parent were tested. Los Angeles Abrasion tests according to ASTM C131-89 were also performed on all four coarse aggregates at 500 revolutions. The results obtained are presented in Table 3.

**Table 3.** Some mechanical properties of the coarse aggregates and rocks

Aggregate type	Compressive strength (MPa)	Modulus of elasticity (GPa)	Abrasion values (%)
Eocene limestone	78	21.5	28.9
Devonian limestone	121	74.3	25.0
Sandstone	156	58.0	17.8
Basalt	238	92.1	15.1

## 2.2 Mixture Design

For each aggregate type, the grading of concrete aggregate was chosen between DIN 1045 A32-B32, closer to B32 and kept constant. Effective water-to-cement ratio, cement content, maximum particle size and aggregate volumes for each concrete class were also kept constant. Since water absorptions of coarse aggregates used were different, in this work, it is considered that the effective water occupies space outside the aggregate particles in the mixture. Each aggregate was in a saturated and surface-dry condition.

Mix proportions of aggregates were kept constant; for normal strength concretes; natural sand: 0.21, crushed sand: 0.19, coarse aggregate No. I: 0.25, coarse aggregate No. II: 0.35. A superplasticizer was used in the high strength concrete class and in order to obtain enough cohesion and workability, the aggregate mix proportions were changed slightly and as a result the proportions for this concrete class were; natural sand: 0.20, crushed sand: 0.16, coarse aggregate No. I: 0.32, coarse aggregate No. II: 0.32. Aggregate gradings were by weight, thus, they varied due to small differences in the specific gravities of the aggregates used. Based on these ratios, calculated aggregate gradings used in the normal strength concretes (NSC) and high strength concretes (HSC) for each aggregate type are given in Tables 4 and 5, respectively.

All mixtures were prepared in a small laboratory mixer with vertical rotation axis by forced mixing.

**Table 4.** Combined aggregate gradings for NSC

Sieve size (mm)	31.5	16.0	8.0	4.0	2.0	1.0	0.5	0.25
Eocene limestone	100	86	57	39	33	29	26	5
Devonian limestone	100	92	55	38	31	28	26	5
Sandstone	100	77	46	39	32	28	24	3
Basalt	100	85	56	39	32	29	25	4

**Table 5.** Combined aggregate gradings for HSC

Sieve size (mm)	31.5	16.0	8.0	4.0	2.0	1.0	0.5	0.25
Eocene limestone	100	87	58	36	31	27	24	4
Devonian limestone	100	93	55	35	29	26	24	4
Sandstone	100	79	43	35	30	26	23	3
Basalt	100	87	57	36	30	27	24	4

The concretes were designated with the following codes: X – EL, X – DL, X – S and X – B. The letter X shows concrete strength (i.e. N for normal strength and H for high strength), and the letters EL, DL, S and B show Eocene limestone, Devonian limestone, sandstone and basalt coarse aggregates, respectively. Details of the mixtures are given in Table 6. For normal strength concretes, air content was varied between 1.0 and 1.3, however, for high strength concretes; this was in the range of 1.8 and 2.3 due to superplasticizer used.

**Table 6.** Mixture proportions (kg/m<sup>3</sup>).

	N-EL	N-DL	N-S	N-B	H-EL	H-DL	H-S	H-B
Cement	279	281	283	281	470	471	477	471
Silica fume	0	0	0	0	47	48	48	47
Water	195	197	198	196	145	145	147	145
Admixture	0	0	0	0	6.3	5.0	6.6	5.9
Natural sand	379	382	385	382	339	341	344	340
Crushed sand	343	358	362	384	271	282	285	302
C.A. (4-16 mm)	448	471	476	507	538	564	571	607
C.A. (8 - 31.5 mm)	631	662	669	712	542	566	573	609
Density	2275	2351	2374	2462	2358	2421	2451	2527
Air (%)	1.3	1.1	1.1	1.0	1.8	2.3	1.8	1.5
Slump(mm)	14	14	14	15	15	14	15	15

C.A.: coarse aggregate

All specimens were kept in their molds for 24 hours. After demolding they were stored in a water tank, saturated with lime at 20°C until 28 days old, followed by laboratory air-curing, until testing at 42 days.

### 2.3 Testing

Compressive strength and modulus of elasticity are measured on five cylindrical specimens of 150 mm in diameter and 300 mm in height. The static moduli of elasticity were calculated from the ascending part of the stress-strain curves in compression for stresses below approximately 30 percent of the ultimate strength using least squares method.

Six cylinders of 150 mm diameter and 60 mm height were used for each concrete mix for the splitting tests.

Three-point bending tests were performed on the beams of 100x100x500 mm size, the support span being 400 mm. The beam specimens contained notches at the mid span which were obtained by cutting with a diamond saw. A notch depth of 17 mm was used in this study. The deflection rate at the middle of the beams was kept constant at 0.02 mm/min. The load was applied by a closed-loop testing machine of 100 kN capacity, and the deflections were measured simultaneously by using LVDTs. Thus, the load versus deflection curve for each beam was obtained by recording measurements taken at the mid point. Crack mouth opening displacements were also recorded. Five beams were tested for each mixture.

To investigate the microstructure of the concretes, plane and thin sections were also prepared. For this purpose; samples of 10 x 20 cm were cut out from the unloaded beam specimens and then impregnated under vacuum with a yellow fluorescent epoxy. Thus, the capillary pores, cracks, voids, and defects in the concrete are filled with epoxy. After impregnation, the plane and thin sections were polished and inspected under UV light using an optical microscope. Microstructural characteristics of the concretes were examined by using an environmental scanning electron microscope (ESEM).

## 3 RESULTS AND DISCUSSION

### 3.1 Strength Properties

#### 3.1.1 Compressive strength

Table 7 presents the strength properties of the concretes produced. As seen in Table 7 and Figure 1, at the normal strength class, the compressive strengths of the mixtures containing Devonian limestone and basalt aggregates are almost identical, which are slightly higher than those of the concretes with Eocene limestone and sandstone aggregates. Concretes containing Devonian limestone and basalt aggregates have higher strength also in high strength class. For this strength class, the strengths of Devonian limestone and basalt aggregate concretes are about 20% higher than Eocene limestone and sandstone aggregate ones. According to Sengul et al. [6], in low- or moderate-strength concretes, Eocene limestone containing concrete had the highest compressive strength. In high strength concretes, however, the compressive strength of basalt containing concrete had the highest value. In high strength concretes, the hysteresis loops of Eocene and Devonian limestone concretes are generally narrower than those of basalt and sandstone concretes. Based on their results, it can be concluded that the irreversible energy up to prepeak stress in compression decreases significantly and the loop becomes narrower with an increase in compressive strength. The brittleness index defined increases substantially with the compressive strength of concrete [6].

**Table 7.** Mechanical properties of concretes

Mix Code	Compressive strength (MPa)	Modulus of elasticity (GPa)	Splitting tensile strength (MPa)
N-EL	36.5	23.7	3.6
N-DL	39.4	30.3	4.2
N-S	36.1	22.9	3.8
N-B	39.4	32.3	3.4
H-EL	86.8	39.6	4.7
H-DL	108.1	48.1	5.4
H-S	88.2	40.3	6.6
H-B	106.9	47.5	6.1

It was well established that the paste-aggregate interface is the weakest link and therefore the mechanical properties of concrete are significantly affected by the properties of the interfacial zone. Surface properties of the Devonian limestone and possibly its mineralogy may play a positive role in both normal and high strength concretes. In HSCs, the compressive strength of concrete with Devonian limestone coarse aggregate is higher than those of the other concretes. Based on the test results, it may be concluded that the strength of the aggregate may be dominant in high strength concretes. In high strength concretes, the matrix stiffness is close to aggregate stiffness, as a result, the probability of crack development through aggregate increases and the properties of aggregate become even more important.

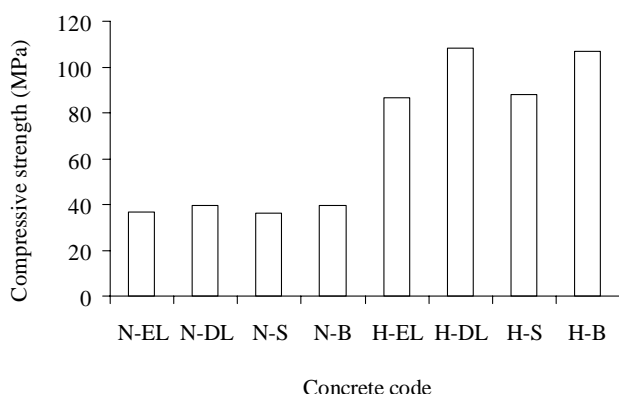


Figure 1. Compressive strength of concretes

### 3.1.2 Modulus of elasticity

Elastic moduli of the concretes investigated are given in Table 7. Similar to the compressive strength test results, concretes containing Devonian limestone and basalt aggregates have higher modulus of elasticity for both normal strength and high strength concrete classes.

For both of the concrete classes, the lower modulus of elasticity of the concretes containing Eocene limestone and sandstone aggregates may be due to the lower elastic modulus of these aggregates (Table 3).

In NSCs, the modulus of elasticity of the concrete with basalt aggregate is approximately 41% higher than that of sandstone. In HSCs, this difference between

the highest (Devonian limestone) and lowest (Eocene limestone) values is approximately 20%. When the aggregate and the cement paste are individually subjected to uniaxial compression, they exhibit an almost linear stress-strain relation. Concrete, however, shows inelastic behavior due to the presence of interfaces between the cement paste and the aggregate. In HSCs, the reduction of the differences between the highest and lowest values of modulus of elasticity may be attributed to the better interfacial zone between cement paste and aggregates at low water/cement ratio. The silica fume used in these concretes may have also helps in strengthening of the interfacial zone.

### 3.1.3 Splitting tensile strength

Splitting tensile strengths of the concretes are also shown in Table 7. In NSCs, the concrete containing Devonian limestone have higher splitting strength. The results of the other mixtures are similar. In HSCs, however, the mixture with sandstone has higher splitting strength.

## 3.2 Fracture Energies

Both ascending and descending branches of the beams were obtained under three point bending loading condition using a closed loop testing machine. Figures 2 and 3 show the typical load – displacement and load – crack mouth opening displacement curves of NSCs, respectively.

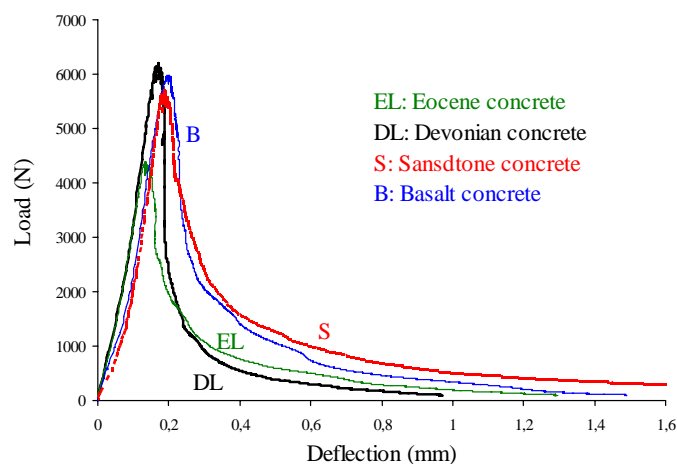
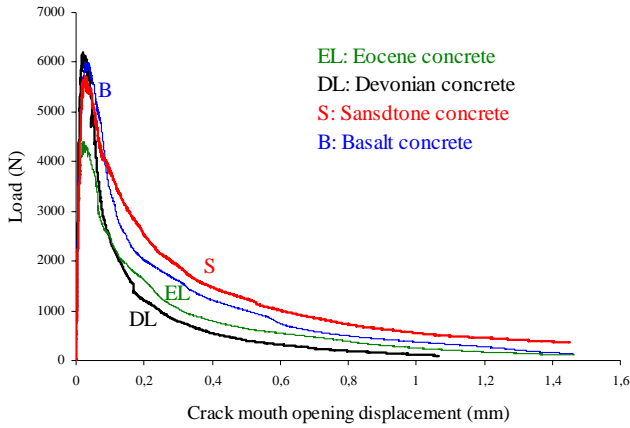
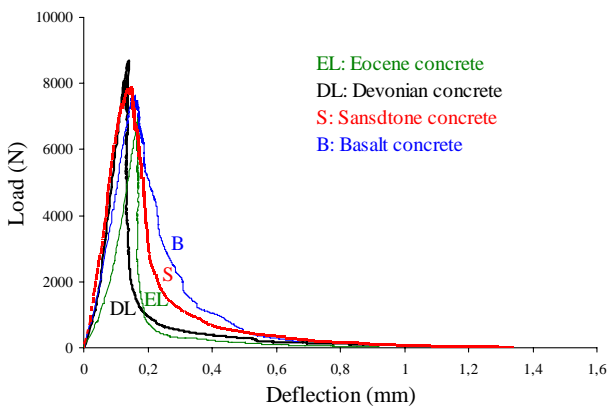


Figure 2. Load – displacement curves for NSCs



**Figure 3.** Load – crack mouth opening displacement curves for NSCs

Typical load versus displacement and load versus crack mouth opening displacement curves obtained for HSCs are given in Figures 4 and 5, respectively.



**Figure 4.** Load – displacement curves for HSCs

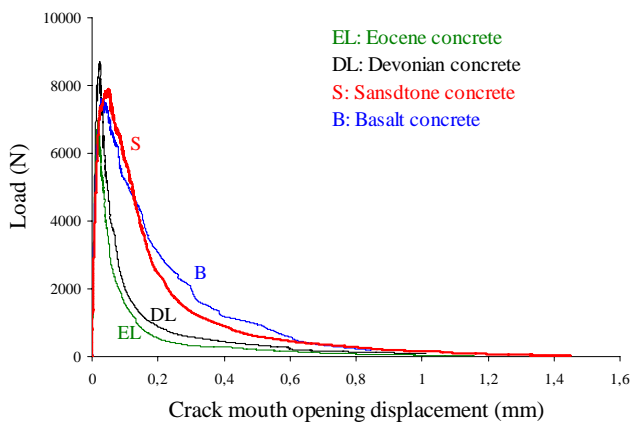


**Figure 5.** Load – crack mouth opening displacement curves for HSCs

The area under each load versus displacement curve is a measure of the fracture energy of the concrete (Figure 6). Based on the test results, fracture energies ( $G_F$ ) of the beams were obtained according to Equation 1:

$$G_F = \frac{W_o + mg\delta_o}{A_{lig}} \quad (1)$$

where  $W_o$  is the area under load versus deflection curve,  $m$  is the mass of the beam,  $g$  is the gravitational acceleration,  $\delta_o$  is the final deflection of the beam and  $A_{lig}$  is the effective cross section of the beam.

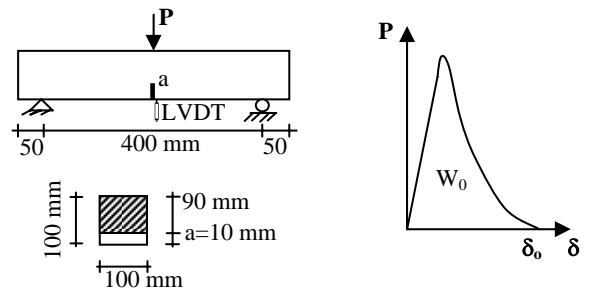


**Figure 6.** Bending test set-up and a typical load versus deflection at mid span curve

From the evaluation of fracture energy ( $G_F$ ), characteristic length ( $l_{ch}$ ) can be calculated as;

$$l_{ch} = \frac{G_F \cdot E}{f_t^2} \quad (2)$$

where  $E$  is the modulus of elasticity and  $f_t$  is the tensile strength of concrete. The results of the bending tests are given in Table 8.

**Table 8.** Fracture properties of concretes

Mix Code	Net flexural strength (MPa)	Fracture energy (N/m)	Characteristic length (mm)
25EL	3.9	97.1	178
25DL	5.2	116.1	199
25S	5.0	210.6	334
25B	4.9	216.9	606
75EL	5.8	80.0	143
75DL	7.4	114.8	189
75S	6.9	200.4	185
75B	6.8	178.5	228

For both of the concrete classes, the flexural strength of the concretes containing Devonian limestone is the highest, and those of the Eocene limestone is the lowest. The surface characteristics may be the possible reason for the higher flexural strength of the concretes with Devonian limestone. Fracture energies of the concrete mixtures are presented in Table 8 and Figure 7. In both concrete classes, concrete produced using basalt coarse aggregate have the highest fracture energy while the mixtures containing Eocene limestone have the lowest fracture energies.

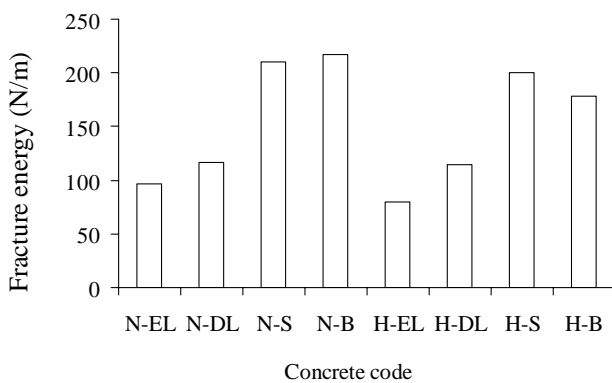


Figure 7. Fracture energies of the concretes

Characteristic lengths of the concretes calculated according to Equation 2, are shown in Table 8 and Figure 8. Characteristic length is a measure of ductility and increase of the characteristic length indicates higher ductility. As seen from the figure, the characteristic length of each concrete at high strength concrete class is lower compared to that of normal strength concrete class.

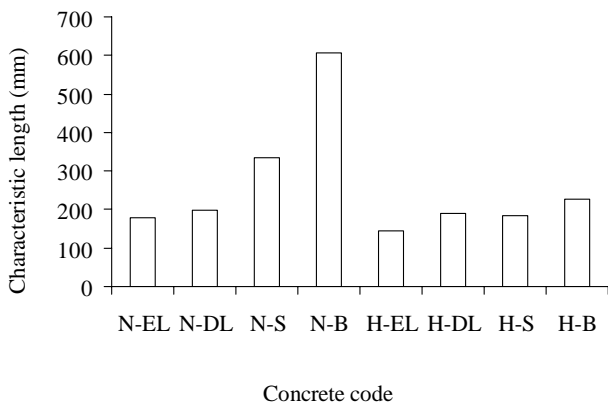


Figure 8. Characteristic lengths of the concretes

### 3.3 Microstructural Investigations

#### 3.3.1 Plane and Thin Sections

To investigate the microstructure of concretes made with different aggregates, plane and thin sections of the concretes were prepared. For this purpose, samples with cross-sectional area of 10 x 20 cm were cut and impregnated with fluorescent epoxy under vacuum. The fluorescent in the epoxy enters the micro-cracks and macro-cracks, capillary, entrained and entrapped air voids, starting from the surface of the specimen. Since the sample is polished and inspected under UV light, it is possible to see the pore structures, and micro- and macro-cracks.

The thin sections give an opportunity to identify the material constituents and estimate their proportions, air content, water-cement ratio, paste homogeneity, paste volume, aggregate volume, effectiveness of curing, and studying the relationships between the various constituents. Figures 9a and 9b show the plane sections of the normal and high strength concretes containing sandstone aggregate under normal light, respectively. Figures 9c and 9d show the same samples under UV light.

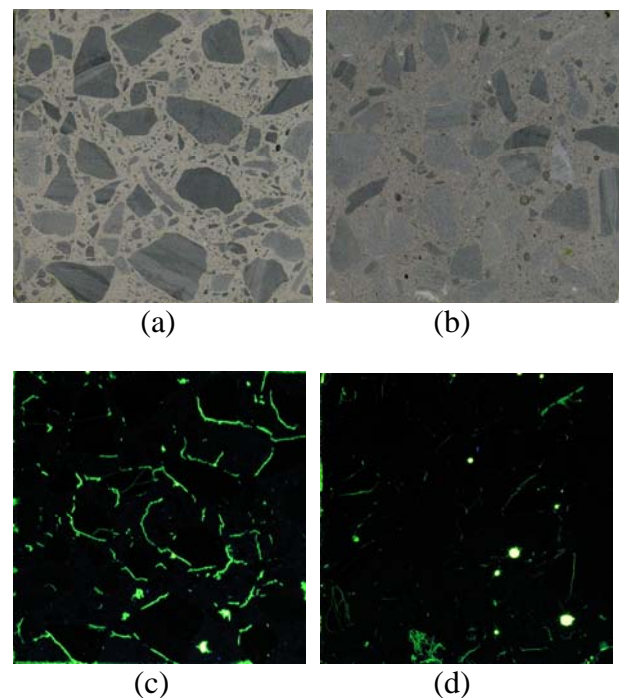
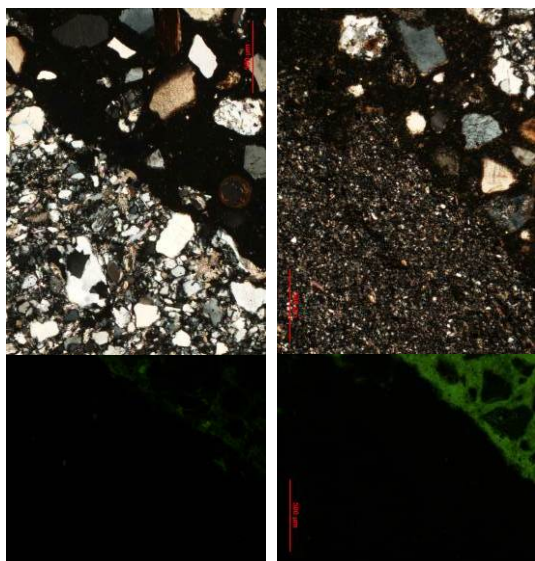


Figure 9. (a) NSC containing sandstone under normal light (b) HSC containing sandstone under normal light (c) NSC containing sandstone under UV light (d) HSC containing sandstone under UV light



As seen in Figure 9c, there are microcracks and pores around the aggregates in the NSCs. In HSCs (Figure 9d), however, only a few microcracks and pores are visible. The bond between paste and aggregates is much better in the latter.

For the thin section analysis, the sample preparations are similar to the ones for the plane section. After impregnation of the specimen with fluorescent epoxy, thin sections are prepared from slices of concrete that are attached to a glass slide, and then ground to a thickness of about 30  $\mu\text{m}$ . Thin section studies also confirmed the better interface characteristics in the HSCs (Figure 10). The aggregates appear as dark, as they do not allow UV-light to pass through. The paste, however appear lighter in color, depending on the capillary pore volume. Due to the low water/binder ratio and use of silica fume in these concretes, the interface between aggregate and hardened cement paste contains less porosity.



**Figure 10.** Crossed polarized (Top) and UV-light (Bottom) thin section views of the HSC (Left) and NSC (Right) mixtures containing sandstone aggregates.

### 3.3.2 Observations under environmental scanning electron microscope

After completion of bending tests, the interfaces between the paste and the aggregates were examined by ESEM. In normal strength concretes, the cracks usually

developed around the coarse aggregate, resulting in a more tortuous and longer fracture path as shown in the Figure 11. In high strength concretes, the cracks usually traversed through the aggregate; transgranular type of fracture was observed, and it was brittle in nature compared to NSCs.

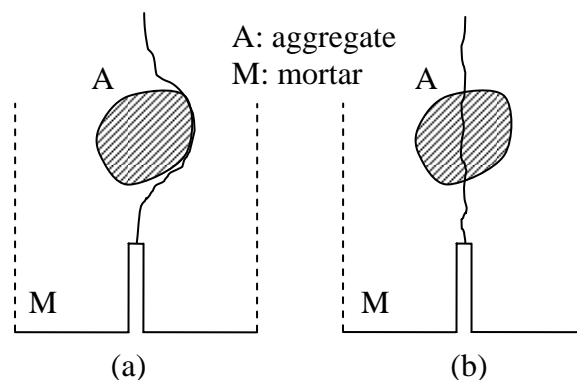


**Figure 11.** Schematic fracture paths (a) NSC (b) HSC

Figure 12 shows that calcium hydroxide (CH) crystals are formed at the paste-aggregate interface of normal strength concretes, as confirmed by other research reports [7-10]. The distribution of CH crystals is mostly tabular, oriented, quite large, and space filling. The calcium silicate hydrate (C-S-H) is also much less dense. The air voids are full with a profusion of CH crystals in the bulk paste. The paste consisted of C-S-H, and the CH is porous.

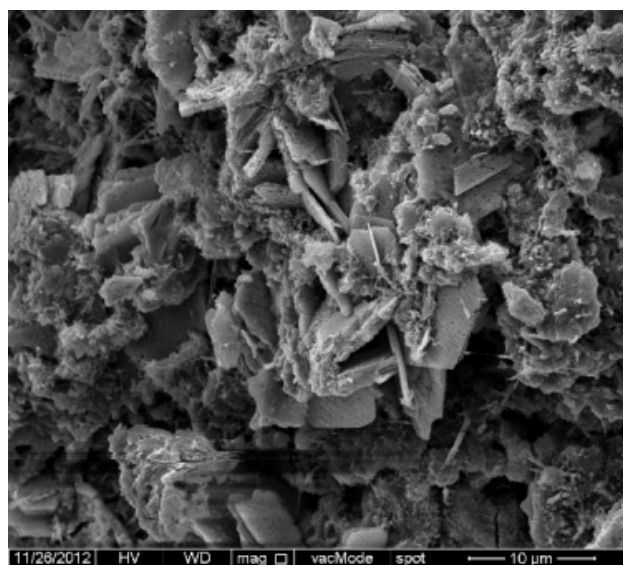


**Figure 12.** Typical SEM micrograph of the aggregate – cement paste interface of the NSC containing sandstone aggregate



As seen in Figure 13, in HSCs, the interfacial zone is composed of dense C-S-H. The air voids and other vacant spaces in this region are empty. CH, monosulfate (AFm), and AFt are not identified in the bulk paste or at the paste-aggregate interface. The paste is dense in the matrix as well as in the interfaces.

The interfacial zone in HSCs is characterized by a direct link between the aggregate and cement paste. As shown in Table 5, silica fume was used in the HSCs. The silica fume reacts with the CH near the aggregate, forming dense C-S-H which fills in the spaces at the interfacial zone, producing increased bond between the paste and aggregate. As a result of this strong bonding, the matrix composed of paste and aggregates act as a composite material and allows transfer of stress more efficiently between the paste and aggregate. Under loading, integral fracture of the entire composite occurs, rather than failure of individual weak components. Thus, concretes with silica fume become stronger, less heterogeneous, denser, with less stress-induced microcracking under loads, and then the fracture occurs in a more brittle manner.

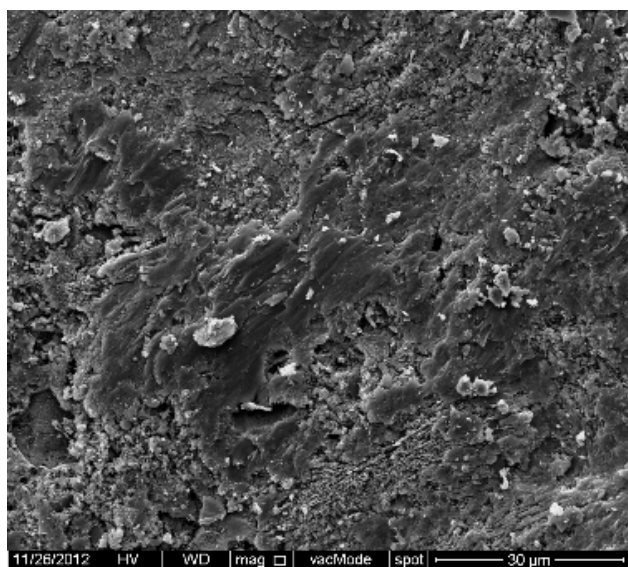


**Figure 13.** Typical SEM micrograph of the aggregate – cement paste interface of the HSC containing sandstone aggregate

### 3.3.3 Comparisons with other micro-structural investigations

The results obtained were compared with other microstructural investigations. Figures 14 and 15 show the SEM micrographs and EDX spectrums in the cement paste for NSC and at the aggregate – cement paste interface for HSC, respectively.

The EDX spectrum at the paste shows a considerably higher Ca peak, which confirms abundant CH crystals in this region. There also some AFt crystals in the same region. This is a characteristic feature of normal concrete not containing any mineral admixture [8]. As seen in Figure 15, dense micro-structure is obtained for HSCs..

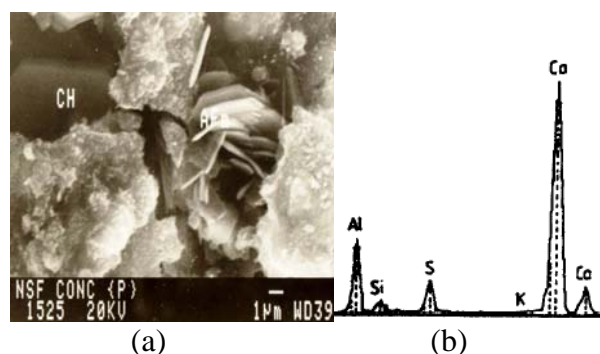


**Figure 14.** (a) SEM micrograph in the cement paste interface of NSC (b) the corresponding EDX spectrum

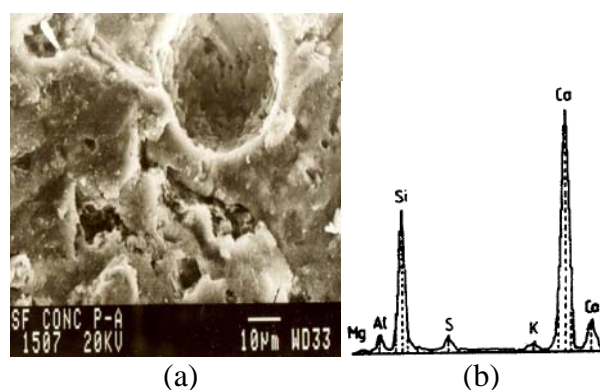


**Figure 15.** (a) SEM micrograph at the aggregate – cement paste interface of HSC (b) the corresponding EDX spectrum

## 4 MODELING OF THE EFFECT OF AGGREGATE

### 4.1 Modeling of Concrete as a Three Phase Composite Material

To determine the influences of the constituents on the stress distributions at the matrix-aggregate interface, around the aggregate and in the matrix close to the aggregate, as shown in Figure 16, a three phase composite material model which consists of a cylindrical model aggregate and a concentric cylindrical shell is proposed by Tasdemir [11].

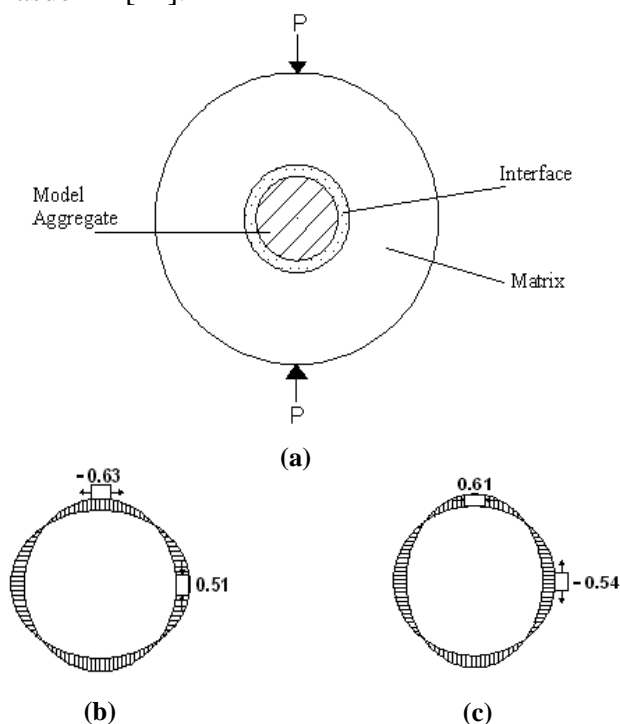


**Figure 16.** Three phase composite model in a disc specimen (a), tangential stress distributions (s.ds.) at the interface in a hard matrix and around a soft inclusion, HSC (b) and, tangential s.ds. at the interface in a soft matrix and around a hard inclusion, NSC (c) [11,12]

According to the details given in Ref. 7 and 8, the model aggregate is located at the center of the disc with the surrounding thin wall matrix-aggregate interfacial zone, and the outer shell as the bulk matrix phase (Figure 16a). Based on the three-phase composite model approach, the following conclusions can be drawn: in high strength concretes, due to the elastic modulus of aggregate being similar

to that of the mortar matrix, the tangential stresses are tensile at the pole and compressive at the equator (Figure 16b), opposite to the results obtained in case of normal strength concrete (Figure 16c). For this reason, cracks are forced to pass through the aggregate which causes the concrete to become more brittle [12].

### 4.2 Model Experiments Previously Published

The three phase composite model was also studied experimentally in previous studies [12]. The objective of these experiments was to investigate the influence of the partial replacement of cement by silica fume on the interface. For this purpose; a model aggregate of diameter 30 mm was embedded in mortar matrix. The mortars were prepared with and without silica fume. The specimens of each mix were tested under diametral compression at 28 days (as in Figure 16a). During these diametral compression disc tests, the strains were measured using strain gauges at the critical points having high values of tangential and radial stresses.

In the soft inclusion case, it is seen that tangential stresses in the matrix close to the interface or at the aggregate surface are higher than those of the hard inclusion cases. In specimens with a hard inclusion, it is observed that high values of tangential, radial and shear stress concentration are developed at the interface due to the large differences in the elastic moduli of the aggregate and mortar matrix. In specimens with a soft inclusion, however, since the elastic modulus of the aggregate is close to that of the mortar matrix, lower stress concentrations occur at the aggregate – matrix interface. The results obtained show that in NSCs (the hard inclusion case) the elastic mismatch of the aggregate and the matrix is significant and large tangential, radial and shear stresses occur at the interface. However, in HSCs, the elastic modulus of the aggregate is close to that of the matrix, hence lower tangential, radial and shear stress concentrations develop and low stress distributions occur at the interface.

These results in these concretes having a much more uniform stress distributions at the interfaces as compared to NSCs [13].

Based on the strain-gauge measurements in the model disc specimens with silica fume, higher tensile strain capacity values were recorded with respect to discs without silica fume. There is also a significant effect of silica fume replacement on the splitting tensile strength [12].

### 4.3 Other Model Experiments for Interface Fracture

In previous studies [14, 15], crack initiation and propagation in rectangular blocks of mortar containing central cracks under compression were studied using the fracture mechanics approach, finite element modeling and quantitative holographic interferometry. In these studies, four different interfacial crack orientation angles were used. It is observed seen that debonding at the aggregate-matrix interface always precedes the initiation of matrix cracking. In another study [16], cracks were initiated at the model aggregate-matrix interfaces and after that were propagated parallel to the applied uniaxial compressive load. These types of experiments may be used for better understanding of NSCs without stronger interfaces.

## 5 CONCLUSIONS

Based on the mechanical properties of NSCs and HSCs, on fracture studies, on the three phase composite material model previously proposed, and on microstructural studies at the aggregate – matrix interfaces using ESEM, the following conclusions can be drawn:

1. Compressive strengths of normal strength concretes are almost identical. In high strength concretes, however, the compressive strengths of Devonian limestone and basalt concretes have the highest values and they are practically identical. Reason is that, in high strength concretes, interfaces between hardened cement paste and aggregate are stronger than those of normal strength

concretes, the strength of aggregate becomes important. Results obtained in these concretes show that the higher compressive strength of the rock, the higher compressive strength of concrete. The slightly low compressive strength in sandstone concrete may be explained by the more irregular shape of sandstone aggregates compared with those of other aggregates.

2. In NSCs, sandstone has the lowest elastic modulus (E). In HSCs, Devonian limestone and basalt give significantly higher E values than sandstone and Eocene limestone.

3. In NSCs, the elastic mismatch of the aggregates and the matrix at the interfaces is substantial. In HSCs, however, the elastic modulus of the aggregate is closer to that of the matrix and tangential stress distributions occur at the aggregate – matrix interface. As a result, in HSCs crack will be forced to pass through the aggregate due to tensile stresses occurring at the pole (at the tip of aggregate) and also high levels of tangential stresses occur in the matrix close to the interface or at the aggregate surface.

4. In concretes without silica fume, abundant calcium hydroxide crystals are observed at the paste-aggregate interface. The air voids are full of platy CH crystals. In HSCs, the interfacial zone is composed of dense C-S-H. The air voids in this region are empty and show no deposition of CH crystals. Dense paste identical to that of the interfacial zone is observed.

5. In NSCs, the softening responses have longer tails those of HSCs. HSCs, have greater peak load and steeper gradients of the softening branch and shorter tails with corresponding lower final displacement values. Slight reduction in both fracture energy and characteristic length is also typical for these concretes. Thus, in HSCs, the characteristic length decreases, brittleness increases, and the material becomes more brittle.

## ACKNOWLEDGEMENTS

In this research; the specimens were produced in Akcansa - Betonsa Technological Center, the mechanical tests were conducted at Istanbul Technical University (ITU), the microstructural part of this work was carried out in National Research Center on Membrane Technologies (MEMTEK) Laboratories at ITU.

## REFERENCES

- [1] Neville, A.M., 2004. *Properties of Concrete*, Pearson Prentice Hall.
- [2] ACI Committee 221, 1996. *Guide for Use of Normal Weight and Heavyweight Aggregates in Concrete*, ACI 221R-96, 29 pp.
- [3] Aitcin, P.C. and Mehta, P.K., 1990. Effect of Coarse Aggregate Characteristics on Mechanical Properties of High Strength Concrete. *ACI Materials Journal*. **88**: 103-107.
- [4] Baalbaki, W., Benmokrane, B., Chaallal, O., and Aitcin, P.C., 1991. Influence of Coarse Aggregate on Elastic Properties of High Performance Concrete. *ACI Materials Journal*. **87**:499-503.
- [5] Giaccio, G. et. al., 1992. High Strength Concretes Incorporating Different Coarse Aggregates, *ACI Materials Journal*. **89**:242-246.
- [6] Sengul, O., Tasdemir, C., and Tasdemir, M.A., 2002. Influence of aggregate type on the mechanical behaviour of normal and high strength concretes. *ACI Materials Journal*. **99**:528-533.
- [7] Sarkar, S. L., 1994. The importance of microstructure in evaluating concrete. In V. M. Malhotra (ed), *Advances in Concrete Technology*, 2nd edition, Ottawa, pp. 125-160.
- [8] Tasdemir, C., 1995. Microstructural effects on brittleness of high-strength concretes, In H. Wittmann (ed.) *Fracture Mechanics of Concrete Structures, In; Proceedings FRAMCOS-2*, F., Aetificatio Publishers, Freiburg, Germany, pp. 125-134.
- [9] Tasdemir, C., 1995. Effect of Silica fume on brittleness of high-strength concretes under compression, *ERMCO 95: 11th European Ready Mixed Concrete Congress*, June 21-23, Istanbul, Turkey, pp. 444-452.
- [10] Struble, L., 1987. Microstructure and fracture at cement paste-aggregate interface, In S. Mindess and S. P. Shah, (eds.) *Bonding in Cementitious Composites*, Materials Research Society Symposium Proceedings, V. 114, pp. 11-20.
- [11] Tasdemir, C., 1995. *Effect of aggregate-cement paste interface on the fracture parameters of high strength concretes*. Ph.D Thesis, Istanbul Technical University, (In Turkish with English Summary).
- [12] Tasdemir, M.A., Tasdemir, C., Akyuz, S., Jefferson, A.D., Lydon, F.D. and Barr, B.I.G., 1998. Evaluation of strains at peak stresses in concrete: a three-phase composite model approach. *Cement and Concrete Composites*, **20**:301-318.
- [13] Bremner, T. W. and Helm, T. A., 1986. Elastic compatibility and the behaviour of concrete. *ACI Journal*, **83**:244-250.
- [14] Tasdemir, M. A., Maji, A. K. and Shah, S. P., 1992. Crack growth in concrete under combined mode I and mode II, *Bulletin of Istanbul Technical University*. **45**:133-164.
- [15] Tasdemir, M. A., Maji, A. K. and Shah, S. P., 1987. Crack propagation in concrete under compression. *Journal of Engineering Mechanics*. ASCE. **116**:137-150.
- [16] Maji, A. K., 1989. *Study of concrete fracture using acoustic emission and laser holography*. Ph.D. Thesis, Northwestern University, Evanston, IL.